

Fragmentation dynamics of nitric oxide induced by low-energy heavy ions

Zhixin Li(李志欣), Kaizhao Lin(林楷钊), Xiaolong Zhu(朱小龙), Zhiliang Li(李志亮), Hang Yuan(苑航), Yong Gao(高永), Dalong Guo(郭大龙), Dongmei Zhao(赵冬梅), Shaofeng Zhang(张少锋), and Xinwen Ma(马新文)
Citation: Chin. Phys. B, 2025, 34 (**5**): 053401. DOI: 10.1088/1674-1056/adbdc0
http://cpb.iphy.ac.cn; http://iopscience.iop.org/cpb

What follows is a list of articles you may be interested in

Vibronic effect study of $^1A_2$ state of H_2O and D_2O

Bei-Yuan Zhang(张倍源), Li-Han Wang(王礼涵), Jian-Hui Zhu(朱剑辉), Wei-Qing Xu(徐卫青), Zi-Ru Ma(马子茹), Xiao-Li Zhao(赵小利), Yong Wu(吴勇), and Lin-Fan Zhu(朱林繁)
Chin. Phys. B, 2024, 33 (**5**): 053401. DOI: 10.1088/1674-1056/ad24d9

Absolute partial and total ionization cross sections of carbon monoxide with electron collision from 350 eV to 8000 eV

Taj Wali Khan, Weizhe Huang(黄伟哲), Enliang Wang(王恩亮), Xu Shan(单旭), and Xiangjun Chen(陈向军)
Chin. Phys. B, 2024, 33 (**4**): 043401. DOI: 10.1088/1674-1056/ad20dd

State-selective charge exchange cross sections in collisions of highly-charged sulfur ions with helium and molecular hydrogen

Xiaolong Zhu(朱小龙), Shucheng Cui(崔述成), Dadi Xing(邢大地), Jiawei Xu(徐佳伟), B. Najjari, Dongmei Zhao(赵冬梅), Dalong Guo(郭大龙), Yong Gao(高永), Ruitian Zhang(张瑞田), Maogen Su(苏茂根), Shaofeng Zhang(张少锋), and Xinwen Ma(马新文)
Chin. Phys. B, 2024, 33 (**2**): 023401. DOI: 10.1088/1674-1056/ad0b01

A theoretical study of fragmentation dynamics of water dimer by proton impact

Zhi-Ping Wang(王志萍), Xue-Fen Xu(许雪芬), Feng-Shou Zhang(张丰收), and Xu Wang(王旭)
Chin. Phys. B, 2023, 32 (**3**): 033401. DOI: 10.1088/1674-1056/ac8340

Integral cross sections for electron impact excitations of argon and carbon dioxide

Shu-Xing Wang(汪书兴) and Lin-Fan Zhu(朱林繁)
Chin. Phys. B, 2022, 31 (**8**): 083401. DOI: 10.1088/1674-1056/ac6336

Fragmentation dynamics of nitric oxide induced by low-energy heavy ions

Zhixin Li(李志欣)[1,2], Kaizhao Lin(林楷钊)[2], Xiaolong Zhu(朱小龙)[2,3,4,†], Zhiliang Li(李志亮)[1,‡], Hang Yuan(苑航)[2], Yong Gao(高永)[2,3], Dalong Guo(郭大龙)[2,3], Dongmei Zhao(赵冬梅)[2,3], Shaofeng Zhang(张少锋)[2,3,4], and Xinwen Ma(马新文)[2,3,4]

[1] *College of Physical Science and Technology, Hebei University, Baoding* 071002, *China*
[2] *Institute of Modern Physics, Chinese Academy of Sciences, Lanzhou* 730000, *China*
[3] *State Key Laboratory of Heavy Ion Science and Technology, Institute of Modern Physics, Chinese Academy of Sciences, Lanzhou* 730000, *China*
[4] *University of Chinese Academy of Sciences, Beijing* 100049, *China*

(Received 12 January 2025; revised manuscript received 26 February 2025; accepted manuscript online 7 March 2025)

We study the fragmentation of NO^{q+} ($q = 2,3$) molecular ions produced by collisions between 96 keV O^{6+} ions and neutral nitric oxide (NO) molecules, using the cold target recoil ion momentum spectrometer (COLTRIMS). The kinetic energy release (KER) for various dissociation channels is obtained. For the channel $NO^{2+} \rightarrow N^+ + O^+$, double-electron capture followed by autoionization of the projectile ions is the dominant process, which can be explained by the recapture of loosely bound electrons into highly excited states of the target. For NO^{3+} trication, two dissociation channels, i.e., (a) $N^+ + O^{2+}$ and (b) $N^{2+} + O^+$, are observed, where channel (b) is the dominant channel. Moreover, for dissociation channels originating from the same parent molecular ion, the dissociation channel with a higher charge for the oxygen ion fragment exhibits a higher most probable KER, which is consistent with studies of CO fragmentation by Rajput *et al.* Additionally, it is observed that as capture stability increases, the average KER shifts to higher values.

Keywords: heavy ion collisions, molecular fragmentation, cold target recoil ion momentum spectroscopy

PACS: 34.50.Gb, 34.80.Ht

DOI: 10.1088/1674-1056/adbdc0 **CSTR:** 32038.14.CPB.adbdc0

1. Introduction

When charged ions collide with neutral molecules, electron transfer, emission processes or both may occur. The produced molecular ions subsequently dissociate into various fragments, which are of great significance for studying fragmentation dynamics. With the advent of reaction microscopes, the kinetic information carried by the fragments produced by fragmentation can be analyzed in greater detail. Over the past few decades, extensive experimental studies have been conducted on the interaction processes between ions and molecules. Molecular targets range from diatomic molecules such as N_2[1,2] and CO,[3–5] to triatomic molecules such as CO_2,[6–8] OCS[9–11] and N_2O,[12,13] and further to polyatomic molecules, biomolecules and clusters such as hydrocarbons[14–16] and amino acids.[17–19] These studies have significantly deepened our understanding of molecular fragmentation. Most of these experiments identified dissociation channels using time-of-flight (TOF) correlations. The momenta of fragment ions can be reconstructed to obtain the kinetic energy release (KER) of the dissociation channels, which unveils the dissociation mechanisms.

However, the influence of different electron loss mechanisms, such as electron transfer and electron emission mentioned above, on the fragmentation dynamics has not been studied in detail. In the collision between Ar^{8+} and N_2, the KER distribution for the dissociation of N_2^{q+} ($q = 3$, 4, 5, 6) strongly depends on the number of autoionized electrons from the projectile. As the number of autoionized electrons decreases, the peak value of the KER shifts towards higher energies. In the collision between Ar^{8+} and CO, different dissociation channels of the same parent molecular ion exhibit distinct KER distributions. For the channel with the O ion fragment with a higher charge state, the peak of the KER is located at a higher energy. These studies indicate that the fragmentation dynamics may be highly dependent on the electron loss mechanism during the collision process. Nitric oxide (NO), one of the commonest diatomic molecules, is a by-product of automobile exhaust, industrial emissions and combustion processes; it reacts with oxygen to generate nitrogen dioxide (NO_2), thus making it an important atmospheric pollutant. In terms of biomedicine, NO can act as a vasodilator with advantageous effects on cardiometabolism. Besides, due to its toxicity to pathogens and tumor cells, researchers have utilized its antimicrobial and anticancer potential to develop NO-based therapeutic strategies. Despite its significance, the physicochemical properties of NO are not well understood.

†Corresponding author. E-mail: zhuxiaolong@impcas.ac.cn
‡Corresponding author. E-mail: phd-lzl@hbu.edu.cn

© 2025 Chinese Physical Society and IOP Publishing Ltd. All rights, including for text and data mining, AI training, and similar technologies, are reserved.

Based on the above results, the present study investigates the fragmentation processes induced by the collision between O^{6+} and NO. The ground state electronic configuration of the NO molecule is $1\sigma^2\ 2\sigma^2\ 3\sigma^2\ 4\sigma^2\ 1\pi^4\ 5\sigma^2\ 2\pi^1$, which features an unpaired electron at the 2π highest occupied molecular orbital, indicating that the neutral NO molecule has an open-shell structure. This unpaired electron makes the ionized NO ion generate various configurations and produce diverse dissociation channels. Previous studies have explored the fragmentation of NO^{q+} ($q = 1,\ 2$) induced by photons, electrons and protons, and its energy curves have been calculated. Our study focused on ion-induced two-body fragmentation of NO^{q+} ($q = 2,\ 3$) which has not been looked at in previous studies.

2. Experimental setup

The experiments were conducted at the EBIS platform at the Institute of Modern Physics, Chinese Academy of Sciences, Lanzhou. Details of the setup are described elsewhere.[20–25] In brief, the O^{6+} ion beam is produced in an electron cyclotron resonance ion source, then charge selected, accelerated to 96 keV, and focused and collimated by a lens and slit before entering the collision chamber. The ion beam collides with supersonic NO gas in the collision chamber. The recoil ions generated in the collision are guided to the position-sensitive detector by an electrostatic field along a Wiley–McLaren type TOF spectrometer, which consists of a 107.5 mm acceleration region and a 215 mm field-free drift region. The scattered ions, which have different charge states after collision, are separated from the O^{6+} ion beam by an electrostatic analyzer downstream from the collision zone. The scattered projectiles are detected by another detector, while the uncollided O^{6+} ion beam is collected by a Faraday cup. In the experiment, the extraction field is 186 V/cm. The recoil ion fragments are in coincidence with the scattered projectile O^{5+} and O^{4+} ions, which ensures that the different electron transfer processes can be selected and separated. The momenta of fragments for two-body dissociation channels can be reconstructed by the recorded time and position information. The condition of momentum conservation is employed to decrease background events.

In this experiment, the collision process of O^{6+} and NO is a low-velocity collision, $v_p = 0.49$ a.u., electron capture is the dominant process and the probability of transfer ionization (TI) is small. TI is defined as when one or multiple target electrons are ionized along with one or multiple electrons being captured in the projectile. When the velocity increases to 1.0 a.u., both the TI process and the electron capture process become contributing processes. Comprehensive analyses of the interactions among various collision processes at slow and intermediate velocities can be found in Refs. [2,26,27]. For convenience in discussion we have ignored the contribution of the TI process in this experiment. The reaction process in this experiment can be represented by the following equation:

$$\begin{aligned} O^{q+} + NO &\rightarrow O^{(q-m)+**\cdots} + N^{r+} + O^{s+} \\ &\rightarrow O^{(q-m+n)+} + ne^-_{An} + \sum_k h\nu_k + N^{r+} + O^{s+} \\ &\quad (C\mathit{m}A\mathit{n}), \end{aligned}$$

where $m = r + s$, with m representing the number of captured electrons. In this context, n denotes the number of autoionizing electrons of the projectile, and k denotes the number of radiative photons. For instance, the C3A1 channel represents a process where triple-electron capture is followed by single projectile autoionization. If no autoionization occurs after multiple electron capture, the excited state of the projectile stabilizes via photon emission, i.e., radiative stabilization. The capture stability increases as the number of autoionizing electrons decreases. For the double-electron capture (DC) scenario, stabilization occurs via radiative emission, and the process is termed true double-electron capture (TDC). In addition, if the DC process is followed by projectile autoionization, it is called the autoionizing double-electron capture (ADC) process.

3. Results and discussion

Figure 1 presents the TOF coincidence spectrum for the first-hit and second-hit fragment ions resulting from the O^{6+}–NO collision. The ion species and corresponding charge states for the first-hit fragments are labeled along the top of the horizontal axis, while those for the second-hit fragments are similarly labeled along the vertical axis. Due to momentum conservation, the two-body dissociation channels appear as sharp island-like distributions with negative slope in the TOF spectrum. Various dissociation channels can be identified in the figure. $N^+ + O^+$, as the most prominent channel, is broader with a surrounding extended region compared with the others; this is attributed to the contribution from multi-body fragmentation processes. Two dissociation channels of NO^{3+} trication, i.e., $N^+ + O^{2+}$ and $N^{2+} + O^+$, with similar shapes are identified. The island-like distributions for NO^{4+} and NO^{5+} are also observed, In this paper, we focus on the two-body dissociation processes of NO^{q+} ($q = 2,\ 3$), including $N^+ + O^+$, $NO^{3+} \rightarrow N^+ + O^{2+}$ and $NO^{3+} \rightarrow N^{2+} + O^+$ channels. The KER distributions and relative branching ratios for these channels have been obtained and are presented in Table 1. The KER values calculated using the Coulomb explosion model are also listed for comparison. Based on the potential energy curves of the molecular ions, the KER corresponds to the energy difference between the point in the Franck–Condon region and the dissociation limit of the molecular ion. This provides valuable insight for associating the observed KER features with specific electronic states of the molecular ion.

Table 1. Relative yield (%) of different capture processes of the O^{6+}–NO collision system and its most probable KER (eV).

Dissociation channel	Final projectile				Coulomb energy (eV)	Relative intensity (%)
	O^{5+}		O^{4+}			
	KER (eV)	Relative intensity (%)	KER (eV)	Relative intensity (%)		
$N^+ + O^+$	9.257	97.6	9.257	2.4	12.52	76.9
$N^{2+} + O^+$	18.5	82.5	17.9	17.5	25.04	15.7
$N^+ + O^{2+}$	23.6	81.3	22	18.7	25.04	7.3

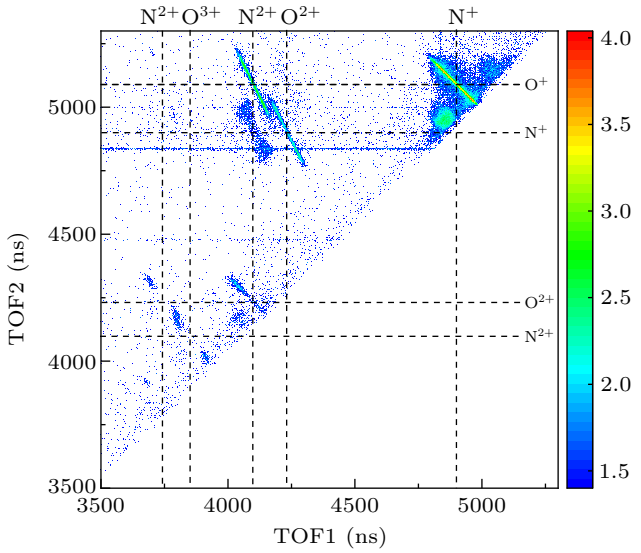


Fig. 1. Time-of-flight correlation spectra of the first- and second-hit ions in O^{6+}–NO collisions at a projectile energy of 96 keV.

3.1. Fragmentation of NO^{2+}

Edvardsson and colleagues studied the process of NO^{2+} fragmentation induced by electron impact and obtained its KER distribution.[28] It extends from 2 eV to 30 eV with a major peak at 9 eV and a sharp peak around 14 eV. Associating the calculated potential energy curves, the electronic states corresponding to different KERs are obtained. In the present work, we investigated the fragmentation of NO^{2+} induced by O^{6+} collisions. The parent molecular ion undergoes dissociation driven by Coulomb repulsion, resulting in singly charged fragments $N^+ + O^+$, which is the dominant dissociation channel observed in this experiment. The experimentally observed KER spectra for the fragmentation of NO^{2+} dications are presented in Fig. 2. The shape of the spectrum is consistent with the KER distribution reported by Edvardsson and colleagues. Two electron loss mechanisms are identified: TDC and ADC processes. The branching ratio of the ADC channel is about 97.6% — this is the dominant process — while the TDC channel contributes only 2.4%. This discrepancy can be interpreted by the recapture of loosely bound electrons into highly excited states of the target. According to the measured KER associated with the potential energy curves (PECs) of NO^{2+} calculated by Edvardsson and colleagues (see Fig. 3), the main peak of the KER distribution can be attributed to the contribution of B $^2\Sigma^+$, C $^2\Sigma^+$, 2 $^4\Pi$, 1 $^4\Sigma^+$, 1 $^4\Delta$ and 1 $^4\Sigma^-$, where the B $^2\Sigma^+$ state pre-dissociates into $N^+(^3P) + O^+(^4S)$, the C $^2\Sigma^+$ state occurs as a tunneling state and dissociates into $N^+(^3P) + O^+(^2D)$ ion pairs, and the crossing of the repulsive state 1 $^2\Delta$ and 2 $^4\Pi$ drives the $N^+(^3P) + O^+(^2P)$ dissociation channel, resulting in an energy release of 9.3 eV. The calculated KER for transitions to the repulsive states 1 $^4\Sigma^+$, 1 $^4\Delta$ and 1 $^4\Sigma^-$ falls within the range of 8–10 eV, which explains why the main peak observed in the experiment appears as a broad and continuous distribution.[28]

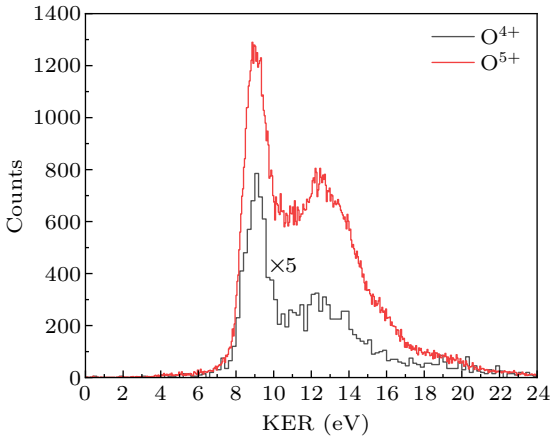


Fig. 2. KER spectra of the $N^+ + O^+$ dissociation channel for different capture-associated processes.

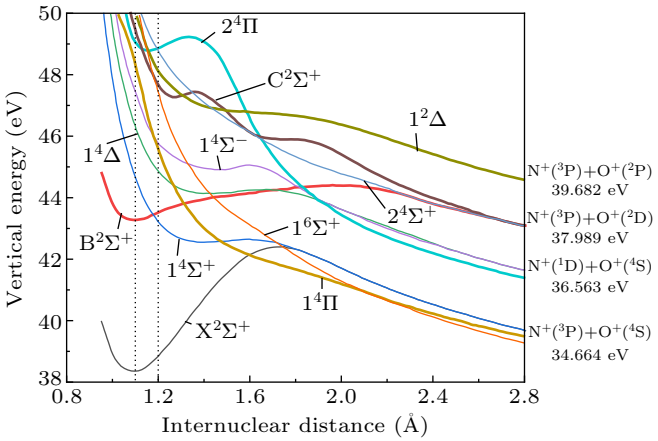


Fig. 3. Potential energy curves for NO^{2+} ions.[28]

3.2. Fragmentation of NO^{3+}

For the NO^{3+} trication, two dissociation channels, i.e., $N^{2+} + O^+$ and $N^+ + O^{2+}$, are observed in the present experiment. Figure 4 shows the KER spectra for the fragmentation of NO^{3+} trications. It is seen that the relative branching ratio

of the $N^{2+}+O^{+}$ channel is about twice that of the $N^{+}+O^{2+}$ channel in Table 1. This discrepancy can be interpreted by the difference in ionization potentials of the participating atoms, where the ionization potential of nitrogen is lower than that of oxygen. The energy required to dissociate into the final states for the two channels is 64.2 eV and 69.7 eV,[29] respectively, resulting in the relative branching ratio of $N^{2+}+O^{+}$ being larger than that of $N^{+}+O^{2+}$.

Figure 5 shows the KER spectra for different electron loss processes in the $N^{2+}+O^{+}$ dissociation channel, which is distinguished by the scattered ions O^{4+} and O^{5+}. The dominant process is triple-electron capture followed by single autoionization (C3A1), with a relative branching ratio of approximately 82.5%, and the most probable KER is 18.5 eV. Another electron loss process involves triple-electron capture followed by double autoionization (C3A2), with a relative branching ratio of 17.5% and a most probable KER of 17.9 eV. The shoulders at higher KER values in both processes mainly originate from the fragmentation of highly excited electronic states. Figure 5(b) presents the KER spectra for the $N^{+}+O^{2+}$ dissociation channel, where C3A1 is also the dominant process, accounting for 81.3%, while C3A2 contributes 18.7%. The most probable KERs for the two processes are 23.6 eV and 22 eV, respectively. In the present experiment, as the capture stability increases from C3A2 to C3A1 the most probable KER shifts to higher values.

PECs are employed to further explain the fragmentation of NO^{3+}. The PECs for the fragmentation of the NO^{3+} trication were also calculated in previous studies.[30] For the $N^{2+}+O^{+}$ channel, the primary contribution to the KER peak comes from the $1\,^{1}\Sigma^{+}$ and $3\,^{1}\Sigma^{+}$ states. The $1\,^{1}\Sigma^{+}$ state couples with the $1\,^{3}\Pi$ state and then dissociates into $N^{2+}(^{2}P)+O^{+}(^{4}S)$, producing a KER of 17.76 eV. The $3\,^{1}\Sigma^{+}$ state can either directly dissociate into $N^{2+}(^{2}P)+O^{2+}(^{2}P)$ with a KER of 20.22 eV or couple with the $2\,^{1}\Pi$ or $3\,^{3}\Pi$ states and dissociate into $N^{2+}(^{2}P)+O^{+}(^{2}D)$, producing a KER of 21.89 eV. However, for the $N^{+}+O^{2+}$ channel, the lack of calculated PECs prevents a further explanation of its KER distribution.

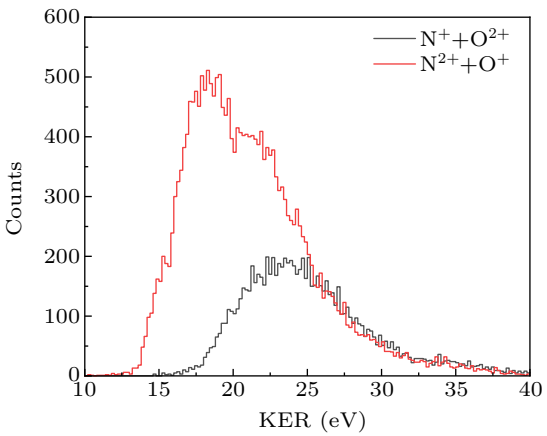


Fig. 4. KER spectrum for NO^{3+} dissociation.

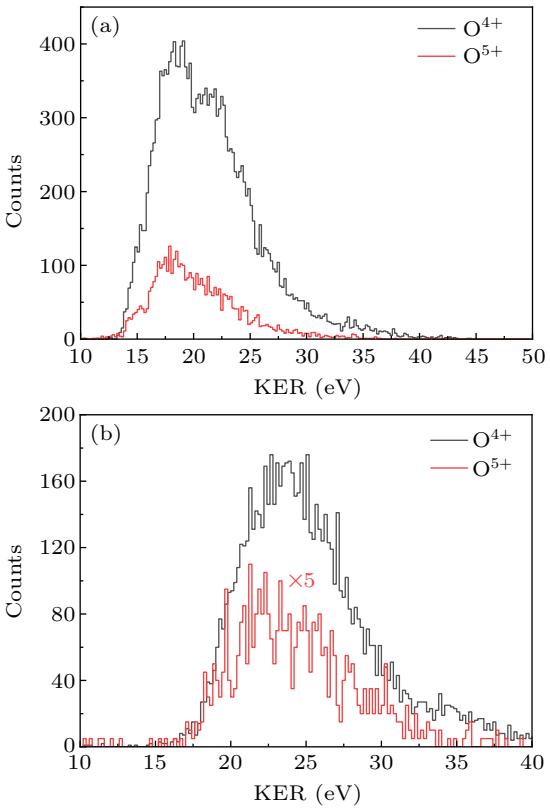


Fig. 5. (a) KER spectra of $N^{2+}+O^{+}$ channels for different capture processes. (b) KER spectra of $N^{+}+O^{2+}$ channels for different capture processes.

4. Conclusions

In this work, we investigated two-body fragmentation of the NO molecule using the cold target recoil ion momentum spectrometer (COLTRIMS). Different dissociation channels are identified and the KER distributions of corresponding channels are obtained. The TOF correlation spectrum directly reveals the dissociation channels for NO^{2+} and NO^{3+}. For the fragmentation of NO^{2+} dications, the ADC process is preferable to the TDC process. The main peak of the KER distribution mainly originates from the $B\,^{2}\Sigma^{+}$, $C\,^{2}\Sigma^{+}$ and $2\,^{4}\Pi$ states. In the case of the NO^{3+} trication, three charges are asymmetrically shared between the two fragments, with a distinct preference for the channel where the nitrogen ion carries a higher charge ($q=2$). Additionally, for dissociation channels originating from the same parent molecular ion it is observed that the most probable KER is higher for the channel where the oxygen ion fragment carries a higher charge. The most probable KER shifts to higher values as capture stabilization increases.

Acknowledgments

Project supported by the National Key Research and Development Program of China (Grant No. 2022YFA1602500), the National Natural Science Foundation of China (Grant Nos. 11934004, 12064040, and 11974358), and Strategic Key

Research Program of the Chinese Academy of Sciences (Grant No. XDB34020000). We acknowledge fruitful discussion with Dr B. Najjari. The authors thank the staff of 320 kV and EBIS platforms for their technical support.

References

[1] Ma J, Li H, Lin K, Song Q, Ji Q, Zhang W, Li H, Sun F, Qiang J, Lu P, Gong X, Zeng H and Wu J 2018 *Phys. Rev. A* **97** 063407

[2] Rajput J, De S, Roy A and Safvan C P 2006 *Phys. Rev. A* **74** 032701

[3] Kaneyasu T, Azuma T and Okuno K 2005 *J. Phys. B: Atom. Mol. Opt. Phys.* **38** 1341

[4] Wells E, Krishnamurthi V, Carnes K, Johnson N G, Baxter H D, Moore D, Bloom K M, Barnes B, Tawara H and Ben-Itzhak I 2005 *Phys. Rev. A* **72** 022726

[5] Rajput J and Safvan C 2007 *Phys. Rev. A* **75** 062709

[6] Folkerts H, Schlathölter T, Hoekstra R and Morgenstern R 1997 *JJ. Phys. B: Atom. Mol. Opt. Phys.* **30** 5849

[7] Neumann N, Hant D, Schmidt L P H, Titze J, Jahnke T, Czasch A, Schöffler M S, Kreidi K, Jagutzki O, Schmidt-Böcking H and Dörner R 2010 *Phys. Rev. Lett.* **104** 103201

[8] Khan A, Tribedi L C and Misra D 2015 *Phys. Rev. A* **92** 030701

[9] Krishnakumar E, Krishnamurthi V, Rajgara F A, Raheja U T and Mathur D 1991 *Phys. Rev. A* **44** R4098

[10] Wales B, Motojima T, Matsumoto J, Long Z, Liu W K, Shiromaru H and Sanderson J 2012 *J. Phys. B: Atom. Mol. Opt. Phys.* **45** 045205

[11] Jana M R, Ghosh P N, Ray B, Bapat B, Kushawaha R K, Saha K, Prajapati I A and Safvan C 2014 *Euro. Phys. J. D* **68** 1

[12] Shen Z, Wang E, Gong M, Shan X and Chen X 2016 *The Journal of Chemical Physics* **145** 234303

[13] Kübel M, Alnaser A S, Bergues B, Pischke T, Schmidt J, Deng Y, Jendrzejewski C, Ullrich J, Paulus G, Azzeer A, *et al.* 2014 *New J. Phys.* **16** 065017

[14] Taylor S, Eland J H D and Hochlaf M 2006 *The Journal of Chemical Physics* **124** 204319

[15] Xu H, Okino T and Yamanouchi K 2009 *The Journal of Chemical Physics* **131** 151102

[16] Xu H, Okino T and Yamanouchi K 2009 *Chemical Physics Letters* **469** 255

[17] Li Y, Xu S, Guo D, Jia S, Jiang X, Zhu X and Ma X 2019 *The Journal of Chemical Physics* **150** 144311

[18] Castrovilli M, Trabattoni A, Bolognesi P, O'Keeffe P, Avaldi L, Nisoli M, Calegari F and Cireasa R 2018 *The Journal of Physical Chemistry Letters* **9** 6012

[19] Zhao J, Song T, Xu M, Quan Q, Siu K M, Hopkinson A C and Chu I K 2012 *Physical Chemistry Chemical Physics* **14** 8723

[20] Zhu X, Ma X, Li J, Schmidt M, Feng W, Peng H, Xu J, Zschornack G, Liu H, Zhang T, *et al.* 2019 *Nuclear Instruments and Methods in Physics Research Section B: Beam Interactions with Materials and Atoms* **460** 224

[21] Ma X, Zhang R, Zhang S, Zhu X, Feng W, Guo D, Li B, Liu H, Li C, Wang J, *et al.* 2011 *Phys. Rev. A* **83** 052707

[22] Xu J, Xu C, Zhang R, Zhu X, Feng W, Gu L, Liang G, Guo D, Gao Y, Zhao D, *et al.* 2021 *The Astrophysical Journal Supplement Series* **253** 13

[23] Yuan H, Xu S, Wang E, Xu J, Gao Y, Zhu X, Guo D, Ma B, Zhao D, Zhang S, *et al.* 2022 *The Journal of Physical Chemistry Letters* **13** 7594

[24] Zhu X, Cui S, Xing D, Xu J, Najjari B, Zhao D, Guo D, Gao Y, Zhang R, Su M, *et al.* 2024 *Chin. Phys. B* **33** 023401

[25] Cui S, Xing D, Zhu X, Su M, Gao Y, Guo D, Zhao D, Zhang S, Fu Y and Ma X 2024 *Chin. Phys. B* **33** 073401

[26] Barat M and Roncin P 1992 *J. Phys. B: Atom. Mol. Opt. Phys.* **25** 2205

[27] Yuan H, Xu Z, Xu S, Ma C, Zhang Z, Guo D, Zhu X, Zhao D, Zhang S, Yan S, Gao Y, Zhang R and Ma X 2022 *Phys. Rev. A* **105** 022814

[28] Edvardsson D, Lundqvist M, Baltzer P, Wannberg B and Lunell S 1996 *Chemical Physics Letters* **256** 341

[29] Fainelli E, Maracci F, Platania R and Avaldi L 1996 *The Journal of Chemical Physics* **104** 3227

[30] Duley A, Dutta N N, Bagdia C, Tribedi L, Safvan C and Kelkar A 2022 *Euro. Phys. J. D* **76** 162